IOP Publishing Journal of Physics: Condensed Matter
J. Phys.: Condens. Matter **32** (2020) 205501 (14pp) https://doi.org/10.1088/1361-648X/ab6cbd

Structural and electronic properties of two-dimensional hydrogenated Xenes

Asad Mahmood and Gul Rahman

Department of Physics, Quaid-i-Azam University, Islamabad 45320, Pakistan

E-mail: gulrahman@qau.edu.pk

Received 1 October 2019, revised 10 December 2019
Accepted for publication 16 January 2020
Published 18 February 2020

Abstract

Structural and electronic properties of pristine two-dimensional group IV Xenes (X = C, Si, Ge, Sn, Pb) and hydrogenated Xenes are studied, using density functional theory (DFT) calculations with and without spin–orbit coupling (SOC). The pristine hexagonal monolayer Xenes show buckled structure upon relaxation except graphene. The buckling δ increases linearly from graphene to plumbene. The band structures without SOC of group-IV Xenes are semi-metallic. However, inclusion of SOC mainly opens the bandgap at the Dirac point. Semi hydrogenation leads to enhanced buckling in all Xenes which indicate a tendency towards more sp^3 like structures. The electronic structures of semi hydrogenated Xenes do not show Dirac cones. Spin polarized band structures show magnetism with magnetic moment of 1.0 μ_B and all SH Xenes are magnetic semiconductor except SH plumbene. Full hydrogenation vanishes buckling upon relaxation and the structure becomes planar implying sp^2-like hybridization. The band structures for fully hydrogenated Xenes turns out to be semiconducting and the Dirac cones also disappear. The bandgap changes from indirect to direct at FH stanene, while FH plumbene turns out to be semi-metallic. SOC gives rise to bandgap of 0.47 eV in FH plumbene, which is otherwise a semi-metal.

Keywords: two dimensional, electronic structures, density functional theory

Supplementary material for this article is available online

(Some figures may appear in colour only in the online journal)

1. Introduction

When it comes to two-dimensional (2D) materials, the likelihood of exploiting their fascinating properties has become an archetype in the quantum world. Dating back to 2004, it is graphene—a honeycomb planar structure of carbon atoms, which is considered a breakthrough in the field of basic science and silicon based electronics as well [1]. Due to free-standing existence of graphene, it is favourably distinguished from its bulk counterpart, graphite. This involves magnificently enhanced electronic properties, specifically the huge carrier mobilities ($\sim 10^6$ m s^{-1}) and strong C–C bonds, which are caused by the electrons bound along the plane behaving as massless Dirac fermions [2]. Nonetheless, these properties sometimes prove to be superfluous for many electron-device applications because of semi-metallic nature of graphene which lacks a bandgap. The characteristically large on–off ratio is always desired in most of the digital devices. The gapless graphene fares poorly on these counts and hence, it is precluded to become a prospective candidate for future generation of nano-electronics. However, the discovery of graphene has evoked an extensive research among scientists to pursue the multi-purpose properties of different 2D materials for electronics, sensors, optoelectronics and catalysis energy storage applications [3, 4]. In an attempt to resolve the bandgap issue of graphene, researchers have been using different techniques, for instance, the chemical functionalization [5–7], applying electric fields [8, 9], strain [10], effect of spin–orbit coupling (SOC) [11], etc. On the other hand, the pursuit for the graphene-like materials has also resulted in a variety of materials ranging from hexagonal boron nitride (hBN), metal monochalcogenides or MMCs (InSe, GaS), transition metal dichalcogenides or TMDCs (MoS_2, MoO_3, $MoSe_2$, WS_2, WSe_2) to other elemental monolayers [12–21].

Just like graphene, hBN is also a planar hexagonal structure with a large bandgap of 5.9 eV, thus, works well as a substrate [12, 13]. Both MMCs and TMDCs are layered structures (held by van der Waals forces) consisting of four and three layers, respectively; each carrying atoms from metals (group III) and chalcogens (group IV and V). So far, many MMCs have been fabricated yet, for instance, InSe and GaS having bandgaps 0.45 eV and 3.4 eV, respectively [22, 23]. Similarly, monolayer of MoS_2 (a typical TMDC) has been reported to show an excellent on–off ratio more than 10^8 to be used as a field-effect transistor (FET) [24, 25]. Additionally, it carries a direct bandgap of 1.8 eV besides a notable carrier mobility. MoS_2 has earned a lot of fame because of its applications in optoelectronics [25], valleytronics [26] and spintronics [27–29]. Despite of tremendously advanced knowledge in the 2D realm, the materials yet speculated or fabricated can not outperform graphene in its transport properties. This can be understood as varied density of states (DOS) and so called 2D nature of these materials at atomic level, as compared to configuration of graphene.

In the recent years, the monolayers (silicene [30], germanene [31], stanene [32, 33], plumbene [34–36]) from group IV elements other than graphene have been hypothesized and chronicled to the elemental 2D literature. For the sake of easiness in frequent use, let us call them Xenes, where X = C, Si, Ge, Sn, Pb. The theoretical studies (including *ab initio* calculations) suggest that these four Xenes possess similar electronic properties as that of graphene, i.e. the presence of Dirac cone. To obtain their monolayer from their bulk phases is not an easy task. In fact, their bulk counterparts do not prefer forming layered structure held by weak van der Waals forces, such as in the case of graphene. Therefore, experimentalists are still unable to achieve their freestanding monolayers, rather they have synthesized these structures as adlayers over the substrates. In the past decade, silicene, germanene, stanene, and plumbene have been epitaxially grown over silver, gold, bismuth telluride, and palladium substrates, respectively [37–40]. Moreover, all the Xenes except graphene are not exactly planar; their structure prefers a little out of plane geometry, which is called buckled structure. The reason of buckling among 2D Xenes is inherited from their corresponding parent 3D structures, which usually prefer sp^3 hybridization of atoms. In fact, the buckling is a mixture of sp^2 and sp^3 hybridized orbitals. It has been theoretically confirmed that two types of buckling, low-buckled and high-buckled, exist among many hexagonal Xenes. For instance, silicene, germanene are energetically more stable in low-buckled phase, while stanene and plumbene prefer high-buckled phase to become more stable—just like closely packed metallic bonds [41–43]. In short, increase in atomic numbers tends the monolayers to be more stable in high-buckled form. The change in buckling height imparts drastic changes on the electronic properties displayed in the band structures.

Spin–orbit coupling has pivotal importance for many phenomena involving spin physics, e.g. spin transport, spin relaxation, quantum spin Hall effect, topological insulators, etc. At atomic level, electron's own spin couples to the magnetic moment arising from the orbital motion of nucleus in electron's frame. In light elements, the strength of SOC is minute such as in graphene [44]. However, in other group IV Xenes, SOC is responsible to open a bandgap [45–48, 50, 51].

Regardless of hardships in their growth, these group IV monolayers earn some advantages over graphene, some of which are following: (1) a strong SOC, which makes it easy to realize the quantum spin Hall effect, (2) tunability of bandgap which is crucial for FET operation, (3) chemically active surfaces which allow bonds with adatoms, and so on. The exceptional findings from experimental analyses and theoretical studies continue to motivate the exploration of other elemental 2D materials, provided their compatibility with the traditional Si based electronics. As an example from group V monolayers, black phosphorene has been successfully fabricated which can exist as a freestanding nanosheet, just like graphene [53]. It is a marvellous semiconductor, holds a superior mechanical flexibility, and its monolayer has a bandgap of 1.88 eV; all of which enable its use as a transistor, as an inverter in optoelectronic devices [53] and in flexible circuits [54].

As has been discussed earlier, chemical functionalization is a proficient tool in engineering the desired properties, specially electronic properties. One of its underlying methods involves surface adsorption by any suitable atom or molecule. Till now, a lot of adatoms have been investigated, most important of which are hydrogen, transition metals and alkali earth metals, halogens, etc. Perhaps the hydrogen adsorption is considered the most common and simplest way of structural modification. Semi-hydrogenated (SH) and fully-hydrogenated (FH) Xenes are the two important conformations of hydrogenating the monolayer Xenes. With these structures, numerous configurations have been tried by the theoreticians including chair, boat, flat and washboard [55–57]. Sluiter and Kawazoe [58] theorized that a chair-like FH graphene could exist due to its dynamic stability, which was later synthesized [59]. Similarly, flat FH silicene was obtained experimentally which also acted as controllable hydrogen storage [60]. On the other hand, theoretical investigations on SH Xenes predict metallic states due to induced ferromagnetism, possibly resulting due to unpaired p_z electron upon semi hydrogenation [61–63]. In 2013, Gmitra and Kochan [64] investigated SOC in SH graphene in two limits: dilute(single H atom in a large supercell) and dense(one H per unit cell). They proposed a model in which band splitting was caused due to local pseudospin inversion symmetry breaking and spin flip. This portrays the novelty of hydrogenation that how H adatom can overturn the physical and electronic structure of otherwise planar and gapless graphene, taking into account the combined effects of SOC, local electric dipoles and symmetry breaking. Likewise, the studies on FH Xenes reveal that that buckling height increases in chair-like FH Xenes which results in sp^3 hybridization. The H adatom removes the p_z states from the Fermi level which results in a wide bandgap opening [59, 65–67]. However, in flat FH Xenes buckling vanishes, causing the flat scafolding, which ends up in increased lattice constant [68, 69]. Furthermore, the band structure of FH Xenes do not show any spin polarized states because of unavailability of unpaired electrons.

Table 1. Optimized lattice constant a (in Å), bond length l (in Å), bandgap E_g (in eV) and cohesive energy E_c (in eV/atom)for the group-IV bulk structures. The values inside brackets represent the previous literature data.

Material	Structure	a	l	E_g	E_c	Category
C	Diamond	3.57(3.57 [76])	1.55	4.15(4.11 [76])	−7.78(−7.78 [77])	Semi-conductor
Si	Diamond	5.47(5.47 [48])	2.37	0.64(0.61 [48])	−4.59(−5.02 [78])	Semi-conductor
Ge	Diamond	5.76(5.76 [79])	2.49	0.00(0.00 [79])	−3.76(−3.76 [80])	Semi-metal
α-Sn	Diamond	6.66(6.65 [81])	2.88	0.00(0.00 [82])	−3.18(−3.20 [81])	Semi-metal
β-Sn	Tetragonal	5.96(5.93 [81])	3.09	0.00	−3.13(−3.16 [81])	Metal
Pb	FCC	5.04(5.05 [83])	3.56	0.00	−3.01(−2.36 [83])	Metal

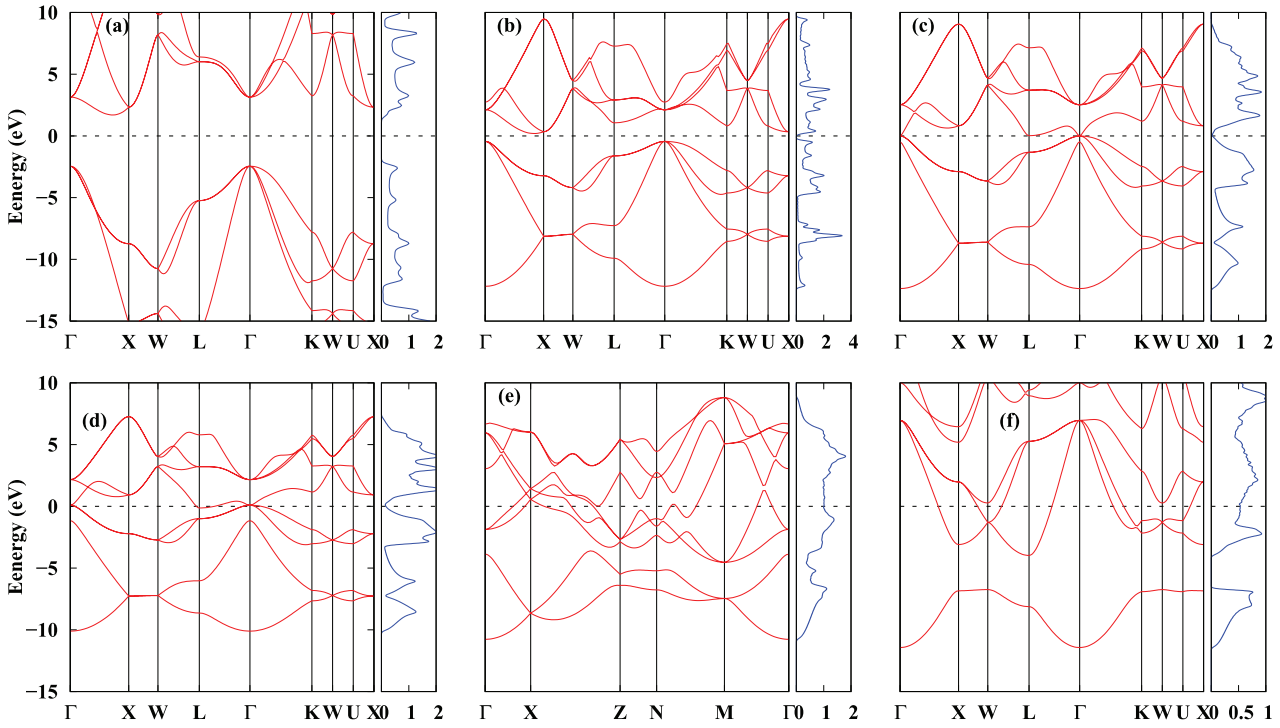

Figure 1. Calculated electronic band structure and total DOS of carbon (a), silicon (b), germanium (c), α-tin (d), β-tin (e), and lead (f). The Fermi level is set to zero eV.

In the light of aforementioned previous work, it is reasonable to presume the need of a thorough investigation to observe how uniformly the geometry and electronic band structure varies in all group-IX monolayers upon hydrogenation. In fact, it would be more intuitive to study these structural trends in terms of the orbitals of bonding electrons. The fact that H atoms can be experimentally adsorbed to only one side of the monolayer further adds to our motivation to study the single-sided hydrogenation. The main purpose of the present work is to investigate and understand the structural and electronic properties of pristine, semi and fully hydrogenated Xenes including SOC.

2. Computational details

We performed full unit cell optimization and electronic structure calculations of pristine, SH and FH Xenes using density functional theory (DFT) with a plane wave basis as implemented in the Quantum ESPRESSO [70] code. We used ultrasoft pseudopotentials [71] and the generalized gradient

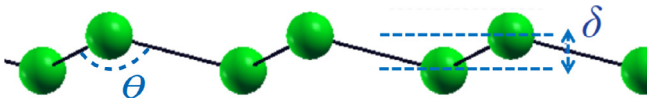

Figure 2. Side view of buckled structure with bond angle θ and buckling height δ.

approximation (GGA) with the exchange-correlation functional of Perdew, Burke, and Ernzerhof (PBE) [72]. The converged value of plane wave basis cut-off was 60 Ry for wave functions and 240 Ry for charge density. A convergence threshold was set at 1×10^{-8} Ry for the energy self-consistency and 0.001 Ry/Bohr for the forces. For the cell relaxation and lattice constant optimization, integration over the Brillouin zone was performed on regular $20 \times 20 \times 1$ Monkhorst–Pack [73] grids, while $30 \times 30 \times 1$ for calculation of DOS, band structures and charge densities. The band structure was plotted along the lines joining high symmetry points, taken in the order: Γ, M, K and Γ. A vacuum gap of about 15 Å is maintained between planes of monolayers to preclude inter-layer interactions.

Table 2. Optimized lattice constant a (in Å), bond length l (in Å), buckling height δ (in Å), degree of hybridization D, bandgap without SOC E_g and with SOC E_g^* (in meV), and cohesive energy E_c (in eV/atom) for the buckled 2D pristine Xenes. The values inside brackets represent the previous literature data.

X	a	l	δ	D	E_g	E_g^*	E_c
C	2.46(2.46 [55])	1.42(1.42 [55])	0.00(0.00 [55])	2.00	0.00	0.00(0.05 [44])	−7.82(−7.95 [85])
Si	3.88(3.87 [86])	2.28(2.28 [86])	0.41(0.45 [86])	2.27	0.00	1.30(1.55 [45])	−3.86(−3.95 [84])
Ge	4.05(4.06 [86, 87])	2.42(2.44 [86, 87])	0.65(0.69 [86],0.67 [87])	2.63	0.00	22.8(23.9 [47])	−3.19(−3.24 [55])
Sn	4.68(4.55 [49],4.67 [55])	2.83(2.75 [49],2.70 [55])	0.85(0.81 [49],0.85 [55])	2.74	0.00	76.2(74.0 [48, 49])	−2.65(−2.8 [88])
Pb	4.94(4.93 [51, 52])	3.00(3.00 [51, 52])	0.93(0.99 [51],0.925 [52])	2.81	0.00	476(440 [51])	−2.28

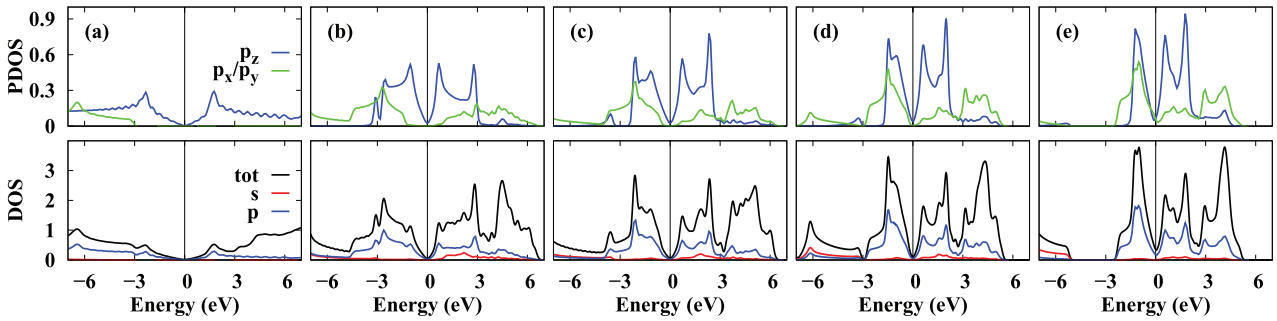

Figure 3. Calculated electronic total DOS (black) and PDOS of pristine graphene (a), silicene (b), germanene (c), stanene (d) and plumbene (e). The zero-axis is set at the Fermi level. The red(blue) color in DOS represents the $s(p)$ contributions. The blue (green) color represents the $p_z(p_x/p_y)$ electrons in PDOS.

3. Results and discussions

In this part, we will discuss the structural and electronic properties of (a) bulk and monolayer Xenes, (b) SH Xenes, and (c) FH Xenes.

3.1. Bulk and monolayer Xenes

Before we present the structural and electronic properties of Xenes, it is very essential to investigate the bulk materials. In this section we present the structural and electronic properties of bulk group-IV elements: carbon, silicon, germanium, tin, and lead. Out of various allotropic forms, we choose to study the diamond structure for C, Si, Ge, and α-Sn. For β-Sn and Pb, we used tetragonal and face-centred cubic structures, respectively. Our calculated equilibrium lattice constant a is 3.57 Å, 5.47 Å, 5.76 Å, 6.66 Å, 5.96 Å, and 5.04 Å for C, Si, Ge, α-Sn, β-Sn, and Pb, respectively. Furthermore, the calculated bond length l is 1.55 Å, 2.37 Å, 2.49 Å, 2.88 Å, 3.09 Å, and 3.56 Å for C, Si, Ge, α-Sn, β-Sn, and Pb, respectively. The cohesive energy E_c per atom of all these materials is also calculated. Our results are summarized in table 1 and our calculated values match well with the previous studies. Table 1 shows that l increases smoothly as one moves from C to Pb. On the other hand, the calculated cohesive energy E_c(per atom) decreases down the group, with a value of -7.78 eV for C, -4.59 eV for Si, -3.76 eV for Ge, -3.18 eV for α-Sn, -3.13 eV for β-Sn, and -3.01 eV for Pb.

Using these optimized structural parameters, we calculated the electronic band structures, total and partial DOS for the above mentioned bulk materials as shown in the figure 1. Note that the band structures of C, Si, Ge and α-Sn look much alike since all of these materials share the same crystal structure. The three-fold degeneracy of the top-most occupied states persists at Γ point for C, Si, Ge and α-Sn (see figures 1(a)–(d)). On the other hand, the calculated band structures for β-Sn and Pb, shown in figures 1(e) and (f), respectively, are different form the aforementioned materials due to their different crystal structures. The resulting bandgap E_g is 4.15 eV for C (semiconductor), 0.64 eV for Si (semi-conductor), 0.00 eV for Ge (semi-metal) and 0.00 eV for α-Sn (semi-metal), where β-Sn and Pb turn out to be metals. To our interest, as we increased the lattice constant of Ge upto 1.8% and calculated the band structure, it resulted into opening the bandgap of 0.49 eV.

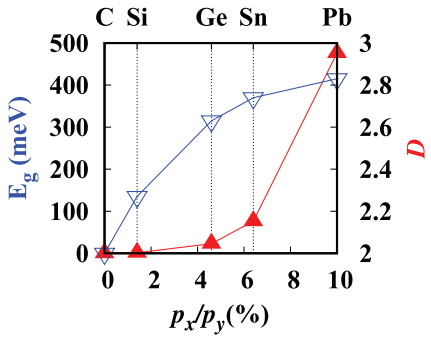

Figure 4. Dependence of E_g (empty triangles) and degree of hybridization D (solid triangles) upon the contribution (%) of p_x/p_y electron to the states at the Fermi level in pristine Xenes.

Disagreement of DFT calculated bandgaps (specially for Si and Ge at equilibrium a) with their experimental values [74] can not be ignored because the error in the results arises due to the fact that GGA does not predict the true electronic bandgaps for most of the semiconducting materials [75]. However, otherwise, these values match well with the previous DFT results (see table 1).

In the above paragraph, we mainly focused on structural and electronic properties of bulk system. It will be very interesting to see how the lattice parameter and electronic structure change when we reduce the dimensionality of a material, i.e. making a monolayer. Here we consider the pristine hexagonal monolayer Xenes of group-IV. Except graphene, all the other group-IV Xenes show buckled structure upon relaxation as shown in figure 2. Our calculated equilibrium lattice constant a, bond length l, and buckling height δ for Xenes are summarized in the table 2. A gradual increase in a, l and δ can be seen as the system changes from graphene to plumbene. The increase in a (or l) can be attributed to atomic radius as one moves down the group—chemical bonds of large atoms tend to equilibrate at larger distances due to electronic repulsion. The emergence of buckling δ observed down the group, which increases as the atomic number of element increases down the group IV element. As the system changes from graphene to silicene, silicene to germanene, and so on, the lattice parameter also increases which results in weakening the bonds between the neighbouring atoms. To regain the bond strength, one of the two atoms (in a unit cell) is forced out of plane, ending up in a buckled structure. And the final structure

Table 3. Optimized lattice constant a (in Å), bond length b/w X_1–X_2 l (in Å), bond length b/w X_1–H h (in Å), buckling height δ (in Å), degree of hybridization D, spin-up (down) bandgap $E_{g_\uparrow}$ ($E_{g_\downarrow}$) in eV, magnetic moment μ (in μ_B/cell), and non-spin polarized (spin-polarized) cohesive energy E_c (E_c^*) in eV/atom for buckled SH Xenes. The values inside brackets represent the previous literature data.

SH-X	a	l	h	δ	D	$E_{g_\uparrow}$	$E_{g_\downarrow}$	μ	E_c	E_c^*
C	2.53(2.53 [64])	1.48(1.49 [61])	1.17(1.16 [61])	0.24(0.32 [61])	2.18	3.23	3.12	1.0	−5.41	−5.47
Si	3.88(3.89 [86])	2.35(2.35 [86])	1.52(1.51 [86])	0.70(0.68 [86])	2.73	2.19	0.90	1.0	−3.16	−3.27
Ge	4.20(4.11 [86, 87])	2.50(2.49 [86, 87])	1.58(1.58 [86, 87])	0.78(0.76 [86], 0.74 [87])	2.84	0.89(0.89 [87])	0.23	1.0	−2.64	−2.72
Sn	4.75(4.11 [63])	2.89(2.89 [63])	1.76(1.76 [63])	0.92(0.92 [89])	2.87	0.54	0.00	1.0	−2.28	−2.32
Pb	4.14	3.09	1.81	1.97	—	—	—	0.0	−2.12	−2.12

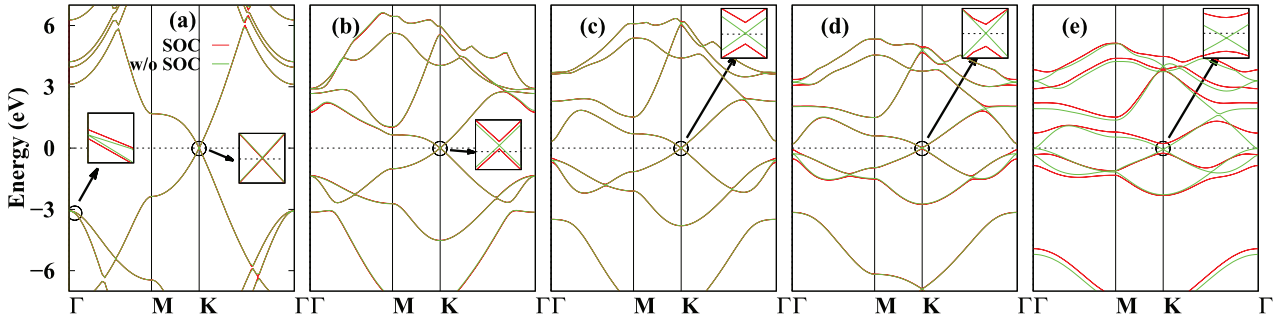

Figure 5. Calculated electronic band structure of pristine graphene (a), silicene (b), germanene (c), stanene (d) and plumbene (e). Red(green) color represents SOC(non-SOC) calculations. The insets show magnified areas of the mentioned portion. The Fermi level is set to zero eV.

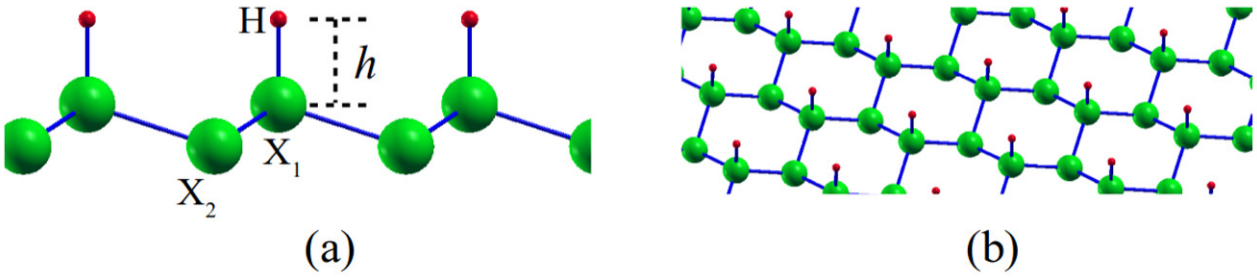

Figure 6. Side (a) and perspective(b) views of a typical SH Xene with an X–H bong length h. Large (small) balls represent X (H) atoms. X_1 (X_2) show the hydrogenated (unhydrogenated) atom.

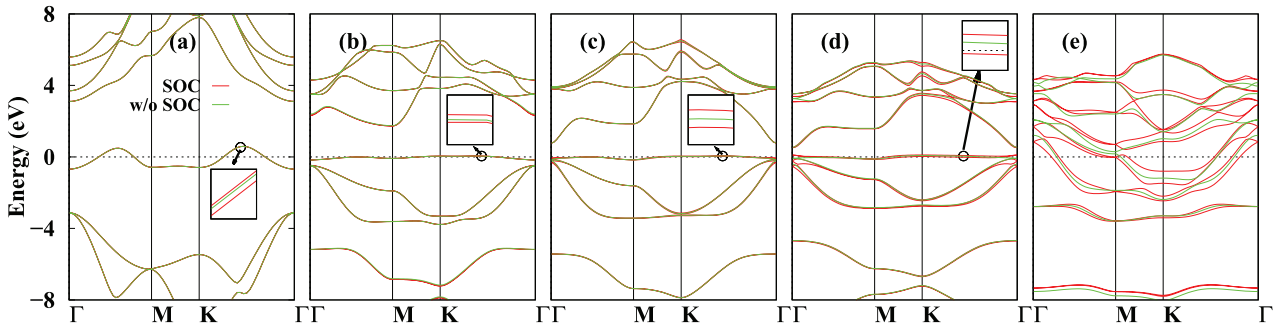

Figure 7. Calculated electronic band structure of non-spin polarized buckled SH graphene (a), silicene (b), germanene (c), stanene (d) and plumbene (e). The insets show magnified areas of the mentioned portion. Red(green) color represents SOC (non-SOC) calculations. The Fermi level is set to zero eV.

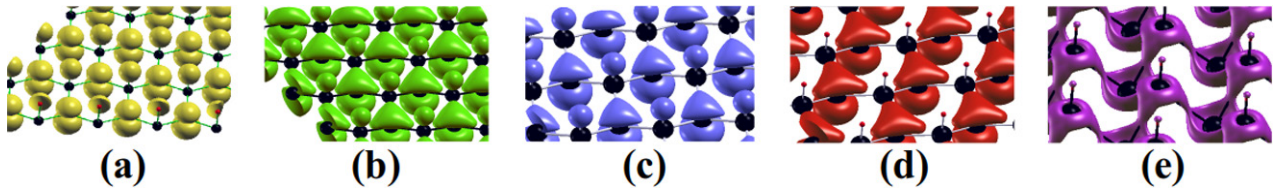

Figure 8. Calculated 3D charge density shown by isosurfaces for SH graphene (a), silicene (b), germanene (c), stanene (d), and plumbene (e).

achieved in this way possesses strong bonds as compared to unrelaxed one. Hence, buckling prompts in most of the monolayers upon relaxation due to their tendency to be more energetically stable. We also studied the planar structures of pristine Xenes (except graphene) and found their optimized lattice constants are larger in magnitude than those of their buckled counterparts because the absence of buckling would bring the nuclei close enough so that they repel each other and attain an enhanced bond length. We also calculated the cohesive energy per atom which is also summarized in table 2, and it is clear to see that the cohesive energy for planar Xenes has smaller values than for buckled ones.

The bond angle θ (see figure 2) between the X atoms can be correlated with the degree of hybridization D, given by the

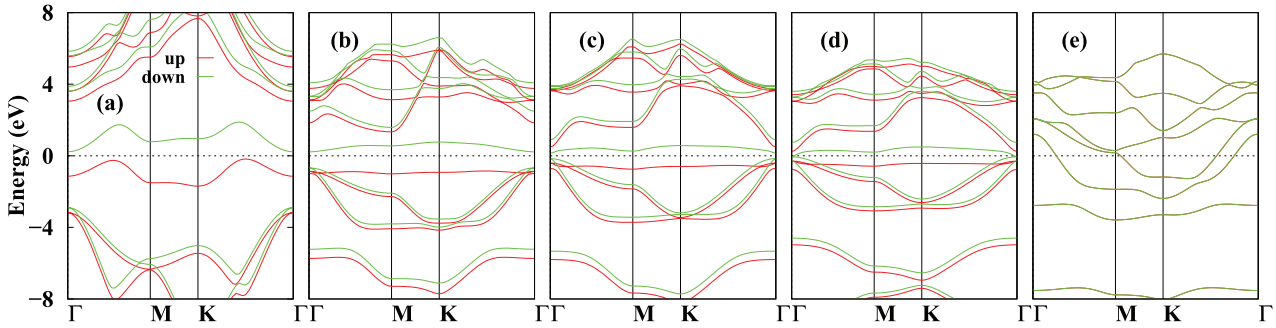

Figure 9. Calculated electronic band structure of spin polarized buckled SH graphene (a), silicene (b), germanene (c), stanene (d), and plumbene (e). Red(green) color represents spin-up(down) calculations. The Fermi level is set to zero eV.

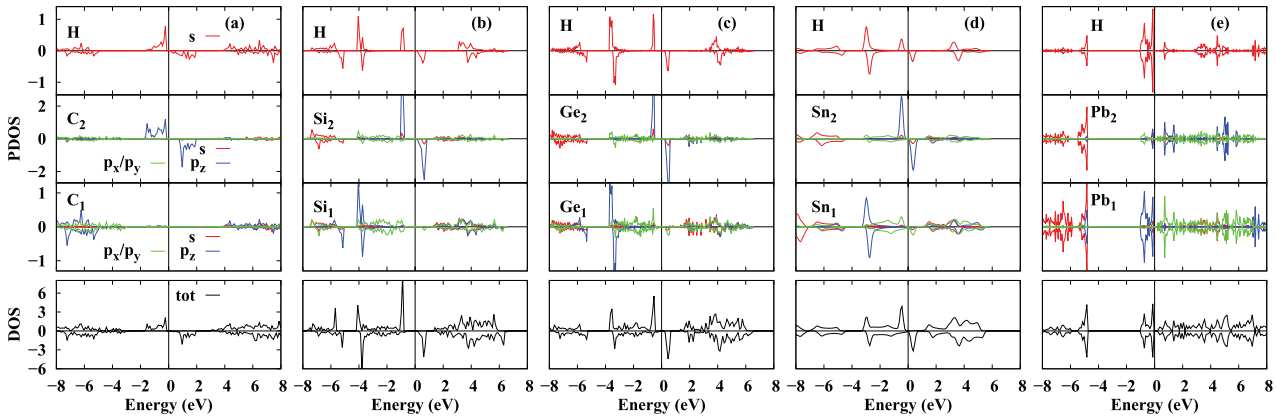

Figure 10. Calculated electronic total DOS (black) and PDOS of spin polarized buckled SH graphene (a), silicene (b), germanene (c), stanene (d), and plumbene (e). The zero-axis is set at the Fermi level. The red(blue) color represents the total $s(p)$ orbital contributions.

empirical relation $D = -1/\cos(\theta)$, which helps to understand the sp^D hybridization [84]. In the case of pristine Xenes, the calculated bond angle uniformly varies from 120° to 110.9° for graphene to plumbene, respectively. This shows that graphene is purely sp^2 while plumbene is almost sp^3 hybridized ($D = 2.81$). In between these two extremes, the D uniformly varies from 2 to 3 for the remaining three Xenes, as shown in table 2. Interestingly, we are successful in representing the dependence of D on the contribution of p_x/p_y electrons to the states at Fermi level. As shown in the figure 3, the calculated projected density of states (PDOS) reveals that the electrons at the Fermi level are purely p_z in case of graphene, resulting in strong π bonds. But in silicene (upto plumbene), p_x/p_y electrons also show their contributions to the top-most filled state in addition to p_z electrons. Thus, the bonds are no longer purely π type, rather a mixing of π and σ bonds. The calculated electron localization function (ELF) for the pristine Xenes confirms the sp^2 and sp^3 orbitals mixing (see figure S2 (stacks.iop.org/JPhysCM/32/205501/mmedia)). Having obtained the required data from PDOS calculations, we plot D as a function of contributions from p_x/p_y electrons in figure 4.

Now we will focus on the electronic structure of Xenes. The calculated electronic band structures are shown in figure 5 with and without SOC. At K-point, the Fermi level is seen to be passing through the middle of two intersecting lines, called Dirac cone—assuming a linear energy dispersion in its vicinity. Each band line is two-fold degenerate due to presence of time-reversal and space-inversion symmetries in the systems under consideration. The band structure shows gapless states for all group-IV Xenes without SOC and behave as semi-metallic in nature. However, the inclusion of SOC engenders the fascinating results in that the bandgap arises gradually from 0 meV (graphene) to 476 meV (plumbene), so the SOC mainly opens the bandgap at the Dirac point. From the PDOS data, we analysed that the bandgap opening is attributed to the involvement of p_x/p_y electrons (in the presence of SOC), in addition to p_z electrons, to the top most filled states near the Fermi level, as shown in figure 4. Consequently, graphene, which has no contributions from p_x/p_y at Dirac point shows zero bandgap with or without SOC. As we move to the other group-IV Xenes, p_x/p_y electron states also add to the p_z states, which then induces a bandgap in the presence of SOC. Hence, it is concluded that bandgap opening at the K-point is attributed to p_x/p_y electrons of Xenes. Furthermore, we also studied the planar Xenes for the sake of comparison. The results showed that planar Xenes prefer increased lattice constant (see table S1) and metallic behaviour (see figure S1).

3.2. Semi hydrogenated Xenes

Now we will focus on SH Xenes, where we applied semi hydrogenation to Xenes which refers to the adsorption of H atom to X_1, leaving X_2 intact (see figure 6). Table 3 shows our optimized structural parameters for SH Xenes. We find that SH leads to enhanced buckling δ in all Xenes upon relaxation, as shown in figure 6. It depicts a tendency towards more sp^3 like

Table 4. Optimized lattice constant a (in Å), bond length b/w X–X l (in Å), bond length b/w X–H h (in Å), buckling height δ (in Å), degree of hybridization D, bandgap without SOC E_g and without SOC E_g^* (in eV), and cohesive energy E_c (in eV/atom) for the FH Xenes. The values inside brackets represent the previous literature data.

FH-X	a	l	h	δ	D	E_g	E_g^*	E_c
C	2.83(2.83 [69])	1.64(1.64 [69])	1.07(1.08 [69])	0.00(0.00 [69])	2	1.40(1.89 [69])	1.40	−4.25(−5.54 [69])
Si	4.15	2.39(2.33 [91])	1.50	0.00(0.00 [91])	2	1.90	1.87	−3.05(−4.43 [69])
Ge	4.34(4.36 [87])	2.51(2.52 [87, 91])	1.56(1.56 [87])	0.00(0.00 [87])	2	1.60(1.7 [87])	1.55	−2.64(−3.77 [69])
Sn	4.99	2.88(2.82 [89])	1.75(1.74 [89])	0.00(0.84 [89])	2	1.33	1.14(0.57 [89])	−2.30
Pb	4.87	3.12	1.85	1.37	—	0.00	0.47	−2.00

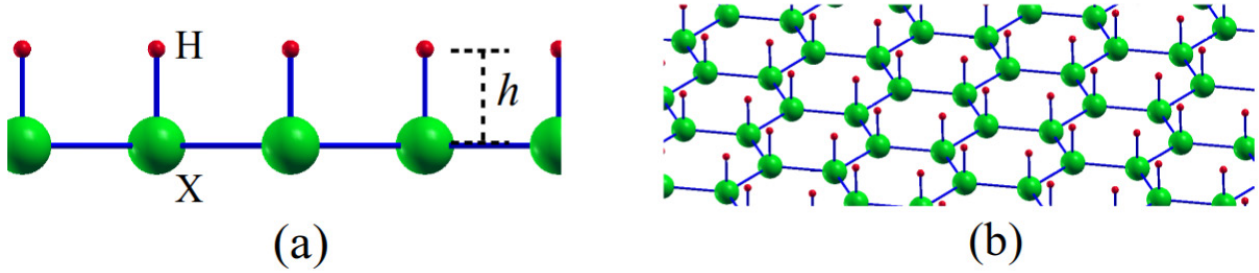

Figure 11. Side (a) and perspective (b) views of a typical FH Xene with an X–H bond length h.

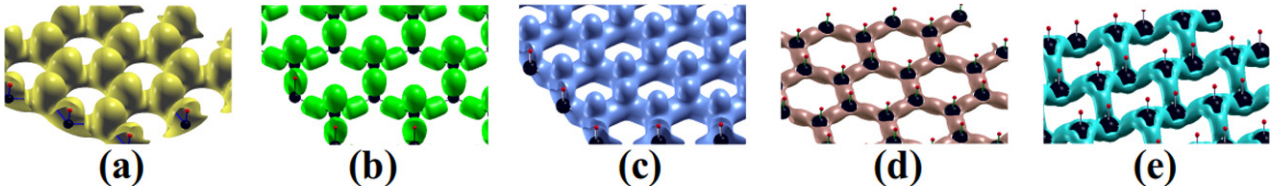

Figure 12. Calculated 3D charge density shown by isosurfaces for FH graphene (a), silicene (b), germanene (c), stanene (d), and plumbene (e).

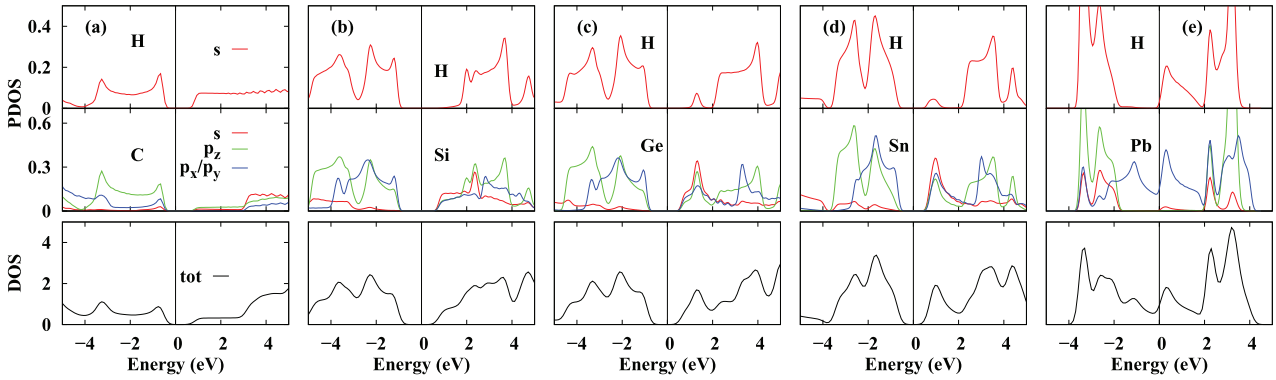

Figure 13. Calculated electronic total DOS (black) and PDOS of FH graphene (a), silicene (b), germanene (c), stanene (d), and plumbene (e). The zero-axis is set at the Fermi level. The red, green and blue colors represent the total s, p_z and p_x/p_y orbital contributions, respectively.

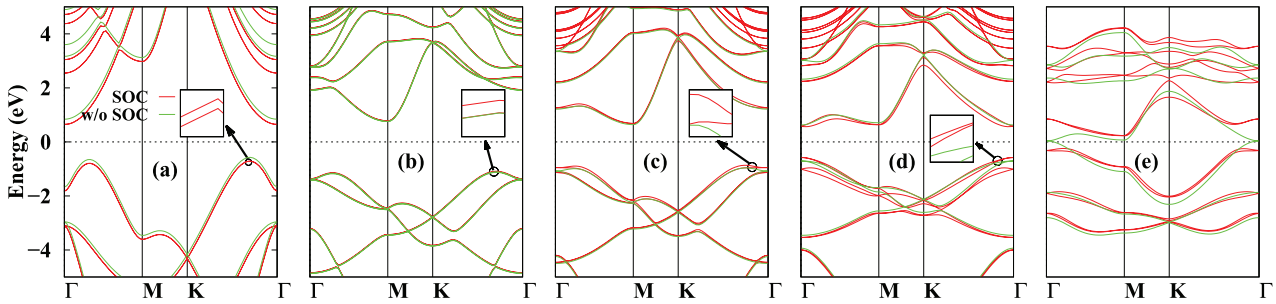

Figure 14. Calculated electronic band structure of FH graphene (a), silicene (b), germanene (c), stanene (d), and plumbene (e). The insets show magnified areas of the mentioned portion. Red(green) color represents SOC(non-SOC) calculations. The Fermi level is set to zero eV.

structures upon semi hydrogenation. Even in the case of graphene which is otherwise planar, semi hydrogenation is capable to pull C atom out of plane. We further observe that the calculated a, l and h for SH Xenes are also increased in magnitude as compared to those of the pristine ones. As a consequence, the computed cohesive energy per atom is also reduced.

As described previously, one of the aspects of this work is to discuss the trends of different properties among Xenes down the group-IV. Again from the table 3, one observes that lattice constant a increases from C to Sn but then decreases for the case of Pb. On the other hand, the bond length l and X_1–H bond length h keep on increasing from C to Pb. This shows that upon SH, the crystal structure of Pb hugely differs from the rest of SH Xenes. To understand this, we come to know from the previous literature that pristine plumbene has two stable structures: low buckled and high buckled. The high buckled structure is much more stable as compared to the low one. We chose to study only the low buckled structure. Since

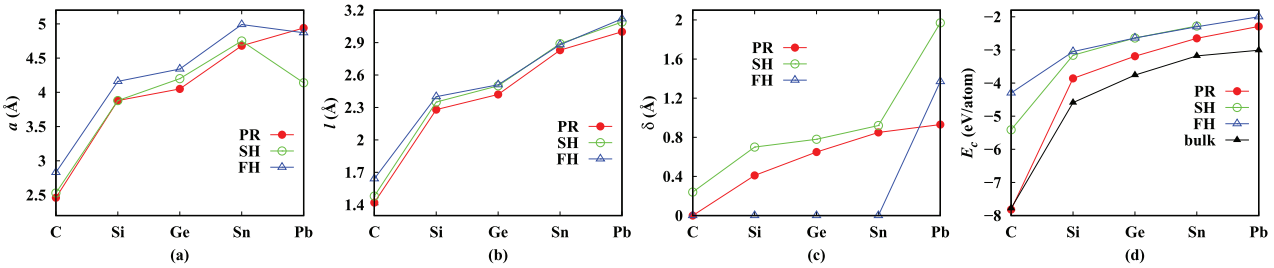

Figure 15. Trends of lattice constant (a), bond length (b), buckling height (c) and cohesive energy (d) among pristine, SH and FH Xenes. Pristine (semi hydrogenated) Xenes are represented by solid (empty) circles, while fully hydrogenated Xenes (bulk phase) are represented by empty (solid) triangles.

it is already comparatively less stable, semi hydrogenation further reduces its stability and the structure distorts tremendously. We will shortly see how deeply the geometry influences the electronic structure of SH Xenes.

The calculated band structures of SH Xenes are shown in the figure 7 in which the top-filled states are seen crossing the Fermi level. As compared to the pristine Xenes, the Dirac cone has now disappeared and flat bands emerge instead. It results because the added H atom makes σ bonds with the host X_1 atom, which ends up breaking the π bonds between p_z orbitals of X_1 and X_2 atoms, as shown in the figure 8. To better visualize the bonds among s, p_x, p_y and p_z orbitals, the calculated ELF is shown in figure S3.

Since hydrogenation breaks the inversion symmetry, we find that incorporating SOC in the non-spin polarized band structure calculations results into splitting of the states, except at time reversal invariant momenta (TRIM) points. The magnitudes of maximum splitting obtained along Γ–K direction are 2 meV, 19 meV, 30 meV, 94 meV and 746 meV from SH graphene to SH plumbene, respectively, which increase down the group. One should note that these values are larger as compared to bandgap opening occurring at K point in case of pristine Xenes. Nevertheless, unlike pristine Xenes, there is no SOC-driven bandgap opening for SH Xenes.

The band at the Fermi energy is mainly contributed by H atoms. Such a band at the Fermi energy will give birth to large DOS at the Fermi energy which will lead to magnetic instability in the system. And it is expected that SH Xenes will show magnetism. The spin polarized band structures are shown in the figure 9. Now it is clear to see a spin polarized band at the Fermi level for all SH Xenes expect Pb which does not show any signature of spin polarization. The absence of spin polarized states is mainly due to structural distortion in Pb.

The spin polarized calculations also yield a magnetic moment of $1.0\mu_B$ due to localized unpaired electron in X_2 atom. Moreover, the spin-up and spin-down states have bandgaps $E_g(\uparrow)$ & $E_g(\downarrow)$, respectively, which decrease down the group as shown in table 3. For spin-up states the bandgap is indirect for SH graphene and SH silicene, and becomes direct bandgap for the rest cases. Similarly, spin-down states show direct bandgap throughout. All direct bandgaps are calculated at Γ point. So SH graphene, silicene, and germanene are magnetic semiconductors and stanene is half-metal whereas plumbene is a non-magnetic metal. The cohesive energies clearly show that the spin polarized states are energetically more favourable than non-spin polarized states.

To know the atomic origin of spin polarization and inducing magnetism in SH Xenes, it is necessary to analyse the PDOS. The PDOS analysis (see figure 10) reveals that the states near the Fermi level mainly consist of p_z electron from X_2 and s electron from H atom. The states from X_2 atoms barely participate towards bonding, however, their contribution show a minute increase as we move down the group upto SH stanene.

One can also see that the spin-up p_z states are completely occupied whereas the spin-down p_z are empty and such occupied and unoccupied states generate large exchange filed that induces magnetism in these systems. Near the Fermi energy, the strong bonding between X_2 and H atoms is also visible. The peaks of X_1 atoms move toward the Fermi energy as one moves from C to Pb. The SH Xenes are found to be energetically less stable as compared to prisitne Xenes, but more stable than planar SH Xenes. The above stated discussion is not valid for SH plumbene due to its distorted structure. However the time reversal (TR) symmetry has now also been broken due to magnetism, hence, the spin polarized band structure always show non-degenerate states at all high symmetry points.

3.3. Full hydrogenated Xenes

Finally, we will discuss fully hydrogenated Xenes. As we fully hydrogenate the Xenes along one side, the buckling vanishes upon relaxation and the structure becomes planar (see figure 11), depicting sp^2 hybridization. This is achieved at the expense of increased lattice constant a and X–X bond length l, both of which are even larger as compared to those of SH Xenes. We must note that buckling in 2D materials strongly depends on the lattice constant, and generally 2D materials with larger lattice constant prefer planar structure than the buckled one [90]. As a result, the cohesive energy E_c of FH Xenes is further decreased, just as anticipated.

Table 4 shows the calculated optimized structural parameters for FH Xenes. As seen in the table 4, the X–X bond length l and X–H bond length h increase for FH Xenes down the group. The values of a, however, only increase till FH stanene followed by a sudden decrease in the value for FH plumbene. We have already seen this type of anomaly in case of SH Xenes, with somewhat similar reason causing this trend in a values down the group. Unlike other FH Xenes, the structure of FH plumbene does not favour planar geometry.

The added H atoms make σ bonds with X atoms causing the π bonds between p_z orbitals of X atoms to become weak. The X–H σ bond strength decreases down the group, as displayed by the charge density (figure 12) and ELF (figure S4 in supplementary information). This fact is evidenced by the PDOS, shown in figure 13 in which the density of p_z states shows a gradual decrease from FH graphene to FH stanene while that of p_x/p_y states remains almost the same. Owing to the difference in geometry of FH plumbene from the rest, its PDOS and charge density show only the existence of p_x/p_y electron states at the Fermi level.

The calculated band structure for FH Xenes turns out to be semiconducting (see figure 14), with a bandgap of the order of eV as shown in table 4. Since π bonding of p_z electrons has lost, the Dirac cone disappears and opens the bandgap E_g. The bandgap is indirect for FH graphene, silicene and germanene, while direct for FH stanene. The FH plumbene turns out to be semi-metallic. The E_g increases as one moves from FH graphene to FH silicene, but then starts decreasing. We also performed the spin polarized calculations and found no signature of spin polarization. The intuition behind this result lies in the unavailability of unpaired localized electrons in any of the X or H atoms. Hence, we conclude that the full hydrogenation mainly changes the electronic structure of Xenes as compared with pristine ones. It is also encouraging to include the SOC in the band structure calculations of FH Xenes. Just like SH Xenes, SOC calculated band structures of FH Xenes also result in splitting of states with magnitudes almost similar to those obtained in case of SH Xenes. Therefore, instead of getting broader, the bandgap E_g^* (as compared to E_g) rather decreases in all FH Xenes (see table 4), except for the case of FH plumbene in which SOC gives rise to bandgap of 0.47 eV, which is otherwise a semi-metal. The band lines split because the system lacks the inversion symmetry, however, the splitting disappears at TRIM points due to TR symmetry.

4. Summary

To summarize, we performed *ab initio* calculations based on DFT to investigate the structural and electronic properties of 2D hydrogenated group-IV Xenes (X = C, Si, Ge, Sn, Pb). The results are summarized in figure 15. We focused on the structural and electronic properties of bulk phases of group IV elements, and we found that both the lattice constant a and bond length l increase as we move down the group-IV except Pb. However, the cohesive energy E_c and bandgap E_g decrease down along the group. The pristine Xenes which showed buckled structure when relaxed except graphene which prefers planar structure. All the Xenes under study, showed gap-less states at the Dirac point. But including SOC opens a bandgap, ranging from a small value of 1.30 meV (silicene) to as large as 476 meV (plumbene). The bandgap of graphene is unaltered by SOC because the states at the Dirac point, are composed of p_z electrons only. We found that p_x/p_y electrons play the key role in removing the degeneracy of states. The planar Xenes showed increased lattice constants and metallic nature, as compared to buckled Xenes.

Upon semi hydrogenation, the relaxed system intensively buckled and became sp^3 hybridized. Even the graphene, which is otherwise planar, showed buckling of 0.24 Å upon hydrogenation. Interestingly found that the bond lengths of SH Xenes enlarged by only 0.6 Å to 0.9 Å more than the corresponding bond lengths of pristine Xenes. It was found that H makes bonds with its next to nearest neighbouring X atoms. In fact, the s electrons of H and p_z electrons of X (unhydrogenated one) are mainly contributed to the states close to the Fermi level. Moreover, spin polarized calculations revealed that the unpaired electron induced a magnetic moment of 1.0 μ_B. We calculated the spin polarized band structure and calculated the bandgaps between spin-up and spin-down states. SH graphene, silicene and germanene fall in the semi-conducting regime while in SH stanene, the spin-down bandgap is closed, therefore, it showed half-metallic nature. As shown in the figure 15(c), the cohesive energies of SH Xenes decrease down the group, with a magnitude less than that of pristine buckled Xenes. On the other hand, the bond length and buckling, both increase down the group(see figure 15).

Fully-hydrogenated Xenes are also considered. The bond length l for all FH Xenes (except graphene) remains more or less the same, compared to those of SH Xenes. The fully hydrogenated systems show planar geometry upon relaxation (except FH plumbene), hence, no buckling arises. The added H atoms strongly bond with the X atoms, which were previously π bonded with each other. Therefore, the Dirac cone is disappeared and a bandgap is opened. The bandgap is indirect and increased from 1.36 eV (FH graphene) to 1.90 eV (FH silicene) and then decreased to 1.60 eV (FH germanene). While FH stanene showed a direct bandgap of 1.33 eV at Γ point. FH plumbene showed semi-metallic nature. The calculated charge density showed no H–H π bonds in all FH Xenes. Rather s electrons from H and p_x/p_y and p_z from X contributed to the bond formation from FH graphene to germanene. But in FH stanene, only p_x/p_y contributed from Sn atom for bond formation. Similar to SH Xenes, the SOC splits the bands in FH Xenes, due to inversion symmetry breaking. However, the SOC results in a bandgap opening for FH plumbene with a value of 0.47 eV. Similar to pristine and SH Xenes, the cohesive energy decreased down the group. We believe that H has much opportunity in Xenes to tune the electronic and structural properties, and Hydrogenated Xenes can be considered for nanoelectronics.

Acknowledgment

We acknowledge the higher education commission (HEC) of Pakistan under the project ‘electronic structure calculations using density functional theory’.

ORCID iDs

Gul Rahman https://orcid.org/0000-0002-5003-4933

References

[1] Novoselov K S, Geim A K, Morozov S V, Jiang D, Zhang Y, Dubonos S V, Grigorieva I V and Firsov A A 2004 Electric field effect in atomically thin carbon films *Science* **306** 666

[2] Novoselov K S, Geim A K, Morozov S, Jiang D, Katsnelson M, Grigorieva I, Dubonos S and Firsov A A 2005 Two-dimensional gas of massless Dirac fermions in graphene *Nature* **438** 197

[3] Balendhran S, Walia S, Nili H, Ou J Z, Zhuiykov S, Kaner R B, Sriram S, Bhaskaran M and Kalantar-Zadeh K 2013 Two-dimensional molybdenum trioxide and dichalcogenides *Adv. Funct. Mater.* **23** 3952

[4] Wang Q H, Kalantar-Zadeh K, Kis A, Coleman J N and Strano M S 2012 Electronics and optoelectronics of two-dimensional transition metal dichalcogenides *Nat. Nanotechnol.* **7** 699

[5] Hildebrand M, Abualnaja F, Makwana Z and Harrison N M 2019 Strain engineering of adsorbate self-assembly on graphene for band gap tuning *J. Phys. Chem.* C **123** 4475

[6] Rahman A U, Rahman G and Kratzer P 2018 Enhanced electronic and magnetic properties by functionalization of monolayer GaS via substitutional doping and adsorption *J. Phys.: Condens. Matter* **30** 95805

[7] Xiao P, Fan X L and Liu L M 2014 Tuning the electronic properties of half-and full-hydrogenated germanene by chlorination and hydroxylation: a first-principles study *Comput. Mater. Sci.* **92** 244

[8] Rahman G 2014 Distortion and electric-field control of the band structure of silicene *Europhys. Lett.* **105** 37012

[9] Avetisyan A A, Partoens B and Peeters F M 2009 Electric field tuning of the bandgap in graphene multilayers *Phys. Rev.* B **79** 035421

[10] Lu Y and Guo J 2010 Band gap of strained graphene nanoribbons *Nano Res.* **3** 189

[11] Yao Y, Ye F, Qi X L, Zhang S C and Fang Z 2007 Spin–orbit gap of graphene: first-principles calculations *Phys. Rev.* B **75** 041401

[12] Novoselov K S, Jiang D, Schedin F, Booth T J, Khotkevich V V, Morozov S V and Geim A K 2005 Two-dimensional atomic crystals *Proc. Natl Acad. Sci. USA* **102** 10451

[13] Park J H *et al* 2014 Large-area monolayer hexagonal boron nitride on Pt foil *Acs Nano* **8** 8520

[14] Xu M, Liang T, Shi M and Chen H 2013 Graphene-like two-dimensional materials *Chem. Rev.* **113** 3766

[15] Hu P *et al* 2013 Highly responsive ultrathin GaS nanosheet photodetectors on rigid and flexible substrates *Nano Lett.* **13** 1649

[16] Demirci S, Avazl N, Durgun E and Cahangirov S 2017 Structural and electronic properties of monolayer group III monochalcogenides *Phys. Rev.* B **95** 115409

[17] Ayari A, Cobas E, Ogundadegbe O and Fuhrer M S 2007 Realization and electrical characterization of ultrathin crystals of layered transition-metal dichalcogenides *J. Appl. Phys.* **101** 014507

[18] Jger-Waldau A, Lux-Steiner M C and Bucher E 1994 MoS_2, $MoSe_2$, WS_2 and WSe_2 thin films for photovoltaics *Solid State Phenom.* **37** 479

[19] Rahman A U, Morbec J M, Rahman G and Kratzer P 2018 Commensurate versus incommensurate heterostructures of group-III monochalcogenides *Phys. Rev. Mater.* **2** 094002

[20] Rahman A U, Rahman G and García-Suárez V M 2017 Development of spontaneous magnetism and half-metallicity in monolayer MoS_2 *J. Magn. Magn. Mater.* **443** 343

[21] Haastrup S *et al* 2018 *2D Mater.* **5** 042002

[22] Millot M, Broto J M, George S, González J and Segura A 2010 Electronic structure of indium selenide probed by magnetoabsorption spectroscopy under high pressure *Phys. Rev.* B **81** 205211

[23] Jung C S, Shojaei F, Park K, Oh J Y, Im H S, Jang D M, Park J and Kang H S 2015 Red-to-ultraviolet emission tuning of two-dimensional gallium sulfide/selenide *ACS Nano* **9** 9585

[24] Chan M Y *et al* 2013 Suppression of thermally activated carrier transport in atomically thin MoS_2 on crystalline hexagonal boron nitride substrates *Nanoscale* **5** 9572

[25] Radisavljevic B, Radenovic A, Brivio J, Giacometti V and Kis A 2011 Single-layer MoS_2 transistors *Nat. Nanotechnol.* **6** 147

[26] Shi H, Pan H, Zhang Y W and Yakobson B I 2013 Quasiparticle band structures & optical properties of strained monolayer MoS_2 and WS_2 *Phys. Rev.* B **87** 155304

[27] Mak K F, McGill K L, Park J and McEuen P L 2014 The valley Hall effect in MoS_2 transistors *Science* **344** 1489

[28] Morpurgo A F 2013 Spintronics: gate control of spin-valley coupling *Nat. Phys.* **9** 532

[29] Xu X, Yao W, Xiao D and Heinz T F 2014 Spin and pseudospins in layered transition metal dichalcogenides *Nat. Phys.* **10** 343

[30] Vogt P, De Padova P, Quaresima C, Avila J, Frantzeskakis E, Asensio M C, Resta A, Ealet B and Le Lay G 2012 Silicene: compelling experimental evidence for graphenelike two-dimensional silicon *Phys. Rev. Lett.* **108** 155501

[31] Ni Z, Liu Q, Tang K, Zheng J, Zhou J, Qin R, Gao Z, Yu D and Lu J 2011 Tunable bandgap in silicene and germanene *Nano Lett.* **12** 113

[32] Zhu F F, Chen W J, Xu Y, Gao C L, Guan D D, Liu C H, Qian D, Zhang S C and Jia J F 2015 Epitaxial growth of two-dimensional stanene *Nat. Mater.* **14** 1020

[33] Liu C C, Jiang H and Yao Y 2011 Low-energy effective Hamiltonian involving spin–orbit coupling in silicene and two-dimensional germanium and tin *Phys. Rev.* B **84** 195430

[34] Zhao H, Ji W X, Zhang C W, Li P, Li F, Wang P J and Zhang R W 2016 First-principles prediction of a giant-gap quantum spin Hall insulator in Pb thin film *Phys. Chem. Chem. Phys.* **18** 31862

[35] Yu X L and Wu J 2018 Evolution of the topological properties of two-dimensional group IVA materials and device design *Phys. Chem. Chem. Phys.* **20** 2296

[36] Yu X L, Huang L and Wu J 2017 From a normal insulator to a topological insulator in plumbene *Phys. Rev.* B **95** 125113

[37] Sone J, Yamagami T, Aoki Y, Nakatsuji K and Hirayama H 2014 Epitaxial growth of silicene on ultra-thin Ag (1 1 1) films *New J. Phys.* **16** 095004

[38] Dvila M E and Le Lay G 2016 Few layer epitaxial germanene: a novel two-dimensional Dirac material *Sci. Rep.* **6** 20714

[39] Saxena S, Chaudhary R P and Shukla S 2016 Stanene: atomically thick free-standing layer of 2D hexagonal tin *Sci. Rep.* **6** 31073

[40] Yuhara J, He B, Matsunami N, Nakatake M and Le Lay G 2019 Graphene's latest cousin: plumbene epitaxial growth on a nano water cube *Adv. Mater.* **31** 1901017

[41] Roome N J and Carey J D 2014 Beyond graphene: stable elemental monolayers of silicene and germanene *ACS Appl. Mater. Interfaces* **6** 7743

[42] Rivero P, Yan J A, García-Suárez V M, Ferrer J and Barraza-Lopez S 2014 Stability and properties of high-buckled two-dimensional tin and lead *Phys. Rev.* B **90** 241408

[43] Lu Y H, Zhou D, Wang T, Yang S A and Jiang J Z 2016 Topological properties of atomic lead film with honeycomb structure *Sci. Rep.* **6** 21723

[44] Boettger J C and Trickey S B 2007 First-principles calculation of the spin–orbit splitting in graphene *Phys. Rev.* B **75** 121402

[45] Lew Yan Voon L C 2016 Physical properties of silicene *Silicene* (Cham: Springer) pp 3–33

[46] Singh R 2018 Spin–orbit coupling in graphene, silicene and germanene: dependence on the configuration of full hydrogenation and fluorination *Bull. Mater. Sci.* **41** 158

[47] Liu C C, Feng W and Yao Y 2011 Quantum spin Hall effect in silicene and two-dimensional germanium *Phys. Rev. Lett.* **107** 076802

[48] Persson K 2013 Materials data on Si (SG:227) by materials project (https://doi.org/10.17188/1190959)

[49] Lu P, Wu L, Yang C, Liang D, Quhe R, Guan P and Wang S 2017 Quasiparticle and optical properties of strained stanene and stanane *Sci. Rep.* **7** 3912

[50] Xiong W, Xia C, Peng Y, Du J, Wang T, Zhang J and Jia Y 2016 Spin–orbit coupling effects on electronic structures in stanene nanoribbons *Phys. Chem. Chem. Phys.* **18** 6534

[51] Li Y, Zhang J, Zhao B, Xue Y and Yang Z 2018 Origin of topologically trivial states and topological phase transitions in low-buckled plumbene (arXiv:1810.02934)

[52] Zhao H, Zhang C W, Ji W X, Zhang R W, Li S S, Yan S S, Zhang B M, Li P and Wang P J 2016 Unexpected giant-gap quantum spin Hall insulator in chemically decorated plumbene monolayer *Sci. Rep.* **6** 20152

[53] Liu H, Neal A T, Zhu Z, Luo Z, Xu X, Tomnek D and Ye P D 2014 Phosphorene: an unexplored 2D semiconductor with a high hole mobility *ACS Nano* **8** 4033

[54] Akinwande D, Petrone N and Hone J 2014 Two-dimensional flexible nanoelectronics *Nat. Commun.* **5** 5678

[55] Balendhran S, Walia S, Nili H, Sriram S and Bhaskaran M 2015 Elemental analogues of graphene: silicene, germanene, stanene, and phosphorene *Small* **11** 640

[56] Pontes R B, Manano R R, da Silva R, Ctica L F, Miwa R H and Padilha J E 2018 Electronic and optical properties of hydrogenated group-IV multilayer materials *Phys. Chem. Chem. Phys.* **20** 8112

[57] Houssa M, Scalise E, Sankaran K, Pourtois G, Afanas Ev V V and Stesmans A 2011 Electronic properties of hydrogenated silicene and germanene *Appli. Phys. Lett.* **98** 223107

[58] Sluiter M H and Kawazoe Y 2003 Cluster expansion method for adsorption: application to hydrogen chemisorption on graphene *Phys. Rev.* B **68** 085410

[59] Elias D C *et al* 2009 Control of graphene's properties by reversible hydrogenation: evidence for graphane *Science* **323** 610

[60] Xu Z, Ao Z, Chu D, Younis A, Li C M and Li S 2014 Reversible hydrophobic to hydrophilic transition in graphene via water splitting induced by UV irradiation *Sci. Rep.* **4** 6450

[61] Zhou J, Wang Q, Sun Q, Chen X S, Kawazoe Y and Jena P 2009 Ferromagnetism in semihydrogenated graphene sheet *Nano Lett.* **9** 3867

[62] Zheng F B and Zhang C W 2012 The electronic and magnetic properties of functionalized silicene: a first-principles study *Nanoscale Res. Lett.* **7** 422

[63] Xiong W, Xia C, Wang T, Peng Y and Jia Y 2016 Strain and spin-orbital coupling effects on electronic structures and magnetism of semi-hydrogenated stanene *J. Phys. Chem.* C **120** 10622

[64] Gmitra M, Kochan D and Fabian J 2013 Spin–orbit coupling in hydrogenated graphene *Phys. Rev. Lett.* **110** 246602

[65] Chen X, Li L and Zhao M 2015 Dumbbell stanane: a large-gap quantum spin hall insulator *Phys. Chem. Chem. Phys.* **17** 16624

[66] Xu Y, Yan B, Zhang H J, Wang J, Xu G, Tang P, Duan W and Zhang S C 2013 Large-gap quantum spin Hall insulators in tin films *Phys. Rev. Lett.* **111** 136804

[67] Pulci O, Gori P, Marsili M, Garbuio V, Del Sole R and Bechstedt F 2012 Strong excitons in novel two-dimensional crystals: silicane and germanane *Europhys. Lett.* **98** 37004

[68] Rong W, Ming-Sheng X and Xiao-Dong P 2015 Chemical modification of silicene *Chin. Phys. Lett.* **24** 086807

[69] Pujari B S, Gusarov S, Brett M and Kovalenko A 2011 Single-side-hydrogenated graphene: density functional theory predictions *Phys. Rev.* B **84** 041402

[70] Giannozzi P *et al* 2009 QUANTUM ESPRESSO: a modular and open-source software project for quantum simulations of materials *J. Phys.: Condens. Matter* **21** 395502

[71] Vanderbilt D 1990 Soft self-consistent pseudopotentials in a generalized eigenvalue formalism *Phys. Rev.* B **41** 7892

[72] Perdew J P, Burke K and Ernzerhof M 1996 Generalized gradient approximation made simple *Phys. Rev. Lett.* **77** 3865

[73] Monkhorst H J and Pack J D 1976 Special points for Brillouin-zone integrations *Phys. Rev.* B **13** 5188

[74] Kittel C 1976 *Introduction to Solid State Physics* vol 8 (New York: Wiley)

[75] Gibson M C, Brand S and Clark S J 2006 Screened-exchange stress tensor in density functional theory *Phys. Rev.* B **73** 125120

[76] Persson K 2014 Materials data on C (SG:227) by materials project (https://doi.org/10.17188/1281384)

[77] Shin H, Kang S, Koo J, Lee H, Kim J and Kwon Y 2014 Cohesion energetics of carbon allotropes: quantum Monte Carlo study *J. Chem. Phys.* **140** 114702

[78] Abdullah B J *et al* 2015 First-principles calculations on cohesive energy of bulk and nano Si *Int. J. Sci. Eng. Res.* **6** 842

[79] Persson K 2016 Materials data on Ge (SG:227) by materials project (https://doi.org/10.17188/1206032)

[80] Farrell H H and Van Siclen C D 2007 Binding energy, vapor pressure, and melting point of semiconductor nanoparticles *J. Vac. Sci. Technol.* B **25** 1441

[81] Legrain F and Manzhos S 2016 Understanding the difference in cohesive energies between alpha and beta tin in DFT calculations *AIP Adv.* **6** 045116

[82] Persson K 2015 Materials data on Sn (SG:227) by materials project (https://doi.org/10.17188/1188292)

[83] Haas P, Tran F and Blaha P 2009 Calculation of the lattice constant of solids with semilocal functionals *Phys. Rev.* B **79** 085104

[84] Cahangirov S, Sahin H, Le Lay G and Rubio A 2016 *Introduction to the Physics of Silicene and other 2D Materials* vol 930 (Berlin: Springer)

[85] Ding Y and Wang Y 2015 Unusual structural and electronic properties of porous silicene and germanene: insights from first-principles calculations *Nanoscale Res. Lett.* **10** 13

[86] Wang X Q, Li H D and Wang J T 2012 Induced ferromagnetism in one-side semihydrogenated silicene and germanene *Phys. Chem. Chem. Phys.* **14** 3031

[87] Liu L, Ji Y and Liu L 2019 First principles calculation of electronic, phonon and thermal properties of hydrogenated germanene *Bull. Mater. Sci.* **42** 157

[88] Modarresi M, Kakoee A, Mogulkoc Y and Roknabadi M R 2015 Effect of external strain on electronic structure of stanene *Comput. Mater. Sci.* **101** 164

[89] Li S S and Zhang C W 2016 Tunable electronic structures and magnetic properties in two-dimensional stanene with hydrogenation *Mater. Chem. Phys.* **173** 246

[90] Rahman G, Mahmood A and García-Suárez V M 2019 Dynamically stable topological phase of Arsenene *Sci. Rep.* **9** 7966

[91] Trivedi S, Srivastava A and Kurchania R 2014 Silicene and germanene: a first principle study of electronic structure and effect of hydrogenation-passivation *J. Comput. Theor. Nanosci.* **11** 781